CrossMark click for updates

Infiltrating monocytes promote brain inflammation and exacerbate neuronal damage after status epilepticus

Nicholas H. Varvel[a,1], Jonas J. Neher[b,c], Andrea Bosch[b,c], Wenyi Wang[a], Richard M. Ransohoff[d], Richard J. Miller[e], and Raymond Dingledine[a]

[a]Department of Pharmacology, Emory University School of Medicine, Atlanta, GA 30322; [b]Department of Cellular Neurology, Hertie Institute for Clinical Brain Research, University of Tübingen, 72076 Tuebingen, Germany; [c]German Center for Neurodegenerative Diseases, 72076 Tuebingen, Germany; [d]Neuro/immunology Discovery Biology, Biogen, Cambridge, MA 02142; and [e]Department of Pharmacology, Northwestern University, Chicago, IL 60611

Edited by Solomon H. Snyder, Johns Hopkins University School of Medicine, Baltimore, MD, and approved July 29, 2016 (received for review March 14, 2016)

The generalized seizures of status epilepticus (SE) trigger a series of molecular and cellular events that produce cognitive deficits and can culminate in the development of epilepsy. Known early events include opening of the blood–brain barrier (BBB) and astrocytosis accompanied by activation of brain microglia. Whereas circulating monocytes do not infiltrate the healthy CNS, monocytes can enter the brain in response to injury and contribute to the immune response. We examined the cellular components of innate immune inflammation in the days following SE by discriminating microglia vs. brain-infiltrating monocytes. Chemokine receptor 2 ($CCR2^+$) monocytes invade the hippocampus between 1 and 3 d after SE. In contrast, only an occasional $CD3^+$ T lymphocyte was encountered 3 d after SE. The initial cellular sources of the chemokine CCL2, a ligand for CCR2, included perivascular macrophages and microglia. The induction of the proinflammatory cytokine IL-1β was greater in FACS-isolated microglia than in brain-invading monocytes. However, *Ccr2* knockout mice displayed greatly reduced monocyte recruitment into brain and reduced levels of the proinflammatory cytokine IL-1β in hippocampus after SE, which was explained by higher expression of the cytokine in circulating and brain monocytes in wild-type mice. Importantly, preventing monocyte recruitment accelerated weight regain, reduced BBB degradation, and attenuated neuronal damage. Our findings identify brain-infiltrating monocytes as a myeloid-cell subclass that contributes to neuroinflammation and morbidity after SE. Inhibiting brain invasion of $CCR2^+$ monocytes could represent a viable method for alleviating the deleterious consequences of SE.

myeloid cell heterogeneity | epileptogenesis | neuroprotection | seizure | microgliosis

Status epilepticus (SE) is a serious medical emergency that triggers a series of cellular and molecular events that can result in the development of epilepsy, a chronic neurological disorder characterized by a persistently lowered seizure threshold (1). The early consequences of SE in rodents include a robust neuroinflammatory response, selective neuronal degeneration, and transient opening of the blood–brain barrier (BBB), leading to later cognitive decline. Although the neuroinflammatory features of SE in man are less well known, extravasation of albumin into the brain was observed for patients who died in SE (2), elevated cerebrospinal fluid levels of the cytokines IL-6, IL-8, and CXCL10 are typically found in patients with refractory SE compared with patients with other inflammatory neurologic disorders (3), and intense gliosis (both astrocytes and microglia) was observed in the temporal cortex of a patient with new-onset focal seizures that progressed to refractory SE (4). These admittedly sparse clinical findings are consistent with the much more extensive animal literature in demonstrating a florid inflammatory response of the brain to SE (5). We and others have provided evidence in animal models of epilepsy that quenching inflammation after SE can provide neuroprotection, prevent BBB opening, alleviate morbidity, and rescue behavioral deficits (6–10).

During some insults to the brain, circulating monocytes can be mobilized to breach the BBB, migrate into the brain, and subsequently contribute to the neuroimmune response in association with microglia (11, 12). Peripheral monocytes are known to enter the brain after traumatic brain injury and contribute to neuronal injury (13), and they play a similar role in multiple sclerosis mouse models (14, 15). In the experimental autoimmune encephalomyelitis (EAE) rodent model of multiple sclerosis, gene-expression profiles indicate that infiltrating monocytes are highly inflammatory compared with microglia. Moreover, invading monocytes induce axonal damage by initiating demyelination, whereas microglia clear debris (16). By contrast, monocytes provide neuroprotection and promote healing after damage to retinal ganglion cells (17) and facilitate recovery after spinal cord injury (18). Taken together, these findings indicate that the net consequence of monocyte infiltration is dependent on disease context. Whether monocytes invade the brain after seizures, and their role in the ensuing highly inflammatory environment, if any, are unknown.

Microglia, the brain's resident innate immune cells of myeloid lineage, actively monitor tissue for injury or pathological alterations (19, 20). Damage to the brain induces microgliosis, a condition characterized by microglia proliferation, morphological transformation, and increased expression of cytokines and chemokines. The microglial population normally maintains itself locally without input from the periphery (21). Traditional techniques of differentiating brain-resident microglia from brain-invading monocytes include the use of bone marrow chimeric animal models. However, this approach is confounded by the i.v. transfer of bone marrow-derived hematopoietic progenitors and irradiation-induced damage to the BBB (21, 22). One evolving method of distinguishing brain-invading monocytes

Significance

Status epilepticus is a frequent neurological emergency. These unabated seizures reduce quality of life, promote the development of epilepsy, and can cause death. Activation of microglia, the brain's resident immune cells, is an invariable feature of seizure activity. However, the involvement of blood-borne immune cells in the brain's inflammatory reaction after seizures remains unresolved. Here we identify a blood cell not normally encountered in the healthy brain, called a monocyte, which invades brain tissue after seizures and contributes to inflammation. Blocking brain entry of the blood monocytes was beneficial, reducing neuronal damage and accelerating weight regain. Treatment strategies aimed at inhibiting peripheral immune cells from entering the brain after seizures could be beneficial.

Author contributions: N.H.V. and R.D. designed research; N.H.V., J.J.N., A.B., and W.W. performed research; R.M.R. and R.J.M. contributed new reagents/analytic tools; N.H.V., J.J.N., R.M.R., R.J.M., and R.D. analyzed data; and N.H.V. and R.D. wrote the paper.

The authors declare no conflict of interest.

This article is a PNAS Direct Submission.

[1]To whom correspondence should be addressed. Email: nvarvel@emory.edu.

This article contains supporting information online at www.pnas.org/lookup/suppl/doi:10.1073/pnas.1604263113/-/DCSupplemental.

from brain-resident microglia is through the chemokine receptor CCR2 (23, 24). A subclass of circulating monocytes expresses high levels of CCR2 (25), whereas microglia lack CCR2 expression (11). Notably, *Ccr2* knockout mice display reduced recruitment of circulating monocytes into inflamed tissues, including the brain, in injury and disease animal models, such as traumatic brain injury (13, 26), EAE models (14, 15), and Alzheimer's disease (27, 28).

Here, we consider the impact of brain-infiltrating $CCR2^+$ monocytes on inflammation and neuronal damage after SE. Additionally, we compare the inflammatory profiles of microglia and monocytes in the brain to evaluate their relative contribution to the innate immune response after SE. Interestingly, the induction of proinflammatory cytokines was greater in microglia than in the invading monocytes, although the basal expression of TNF-α and IL-1β were much higher in monocytes than microglia. Thus, limiting monocyte recruitment into the brain was neuroprotective, reduced opening of the BBB, and accelerated functional recovery, indicating that therapies designed to limit $CCR2^+$ monocytes from entering the brain after SE could be of therapeutic value.

Results

Systemic Administration of Kainic Acid Induces Neurodegeneration, Inflammation, and Delayed Monocyte Infiltration. To determine whether circulating CCR2-expressing monocytes infiltrate the brain after SE, heterozygous $Ccr2^{+/rfp}$ mice were injected intraperitoneally with saline solution or a single dose of kainic acid (KA; 30 mg/kg). Seizure severity was recorded every 5 min for 5 h according to a Racine scale modified for KA (Fig. 1*E*). Brain tissue was examined histologically for evidence of hippocampal neural degeneration, microgliosis, and invasion of circulating monocytes at 1, 3, and 14 d after KA administration. In comparison with saline solution-treated animals, mice that entered SE showed robust thinning and destruction of the pyramidal cell layer in the CA3 subfield of the hippocampus via cresyl violet staining, indicating neuronal degeneration at time points examined (Fig. 1*A*). These data confirm the well-recognized CA3 damage after systemic KA (29, 30). In the saline solution-treated mice, microglia that express ionized calcium binding adapter molecule 1 (Iba1) were evenly distributed throughout hippocampal tissue, with thin, long processes extending away from the cell soma. In contrast, the $Iba1^+$ myeloid cells encountered in mice that entered SE showed a very different pattern consisting of cellular clustering around the damaged neurons and displaying shortening and thickening of their processes at each time point (Fig. 1*A*). Anti-red fluorescent protein (RFP) staining of adjacent brain sections revealed substantial numbers of CCR2-RFP–expressing monocytes in the hippocampus of SE mice 3 d after SE, but not in saline solution-treated controls or in animals subject to KA at the 1-d and 14-d time points (Fig. 1*A*).

Stereological analysis of $Iba1^+$ cells in the hippocampus of saline solution-treated control mice showed approximately 4.7×10^4 cells. One day after SE, the number of hippocampal $Iba1^+$ cells increased to 8.8×10^4 cells, and further increased to 1.7×10^5 cells at the 3-d and 14-d time points (Fig. 1*B*). We found only an occasional $CCR2^+$ cell at the 1-d and 14-d time points. In contrast, 8.0×10^4 $CCR2^+$ monocytes were found in the hippocampus 3 d after SE (Fig. 1*C*). Thus, 3 d after SE, there were approximately equal numbers of activated microglia and monocytes in hippocampus.

To verify that brain-invading $CCR2\text{-}RFP^+$ cells are monocytes and not lymphocytes, such as T cells or natural killer cells, we investigated the expression patterns of the myelomonocytic marker CD11b. As expected, CCR2-RFP–expressing cells were predominantly $CD11b^+$, with few to no appendages extending from the cell soma (Fig. 1*D*, arrows). $CCR2\text{-}RFP^+$, $CD11b^-$ cells that are likely T lymphocytes, were only rarely observed within the monocytic infiltrate (Fig. 1*D*, arrowhead). As expected, we also observed $CD11b^+$ cells with highly ramified morphology, typified

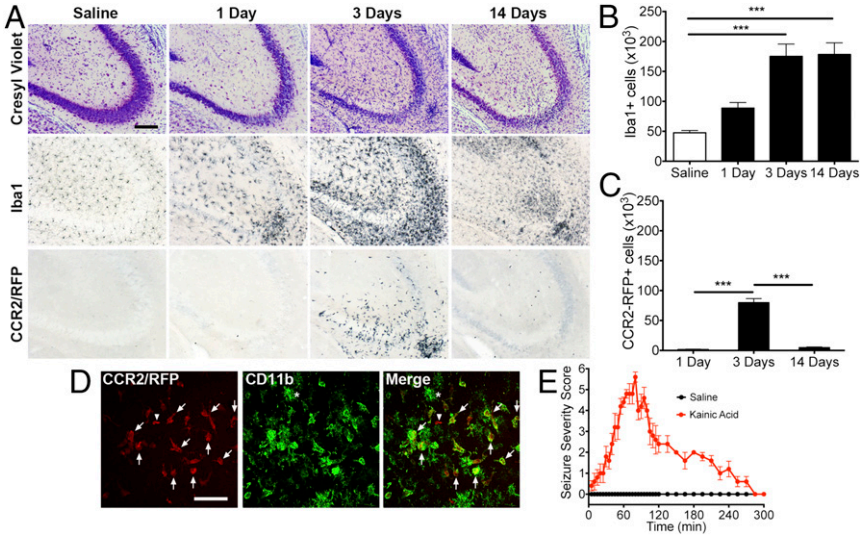

Fig. 1. Hippocampal cell loss and microgliosis precede infiltration of $CCR2^+$ monocytes. Two-month-old CCR2-RFP male mice received intraperitoneal KA (30 mg/kg) or saline solution control injection and were killed 1, 3, or 14 d later. (*A*) The mice subject to KA showed neuronal cell loss in the CA3 hippocampal region at all time points examined. This was accompanied by microgliosis, which was robust at the 3-d time point. Anti-RFP immunohistochemistry revealed isolated $CCR2\text{-}RFP^+$ cells at the 1- and 14-d time points. The 3-d time point showed massive infiltration of $CCR2\text{-}RFP^+$ monocytes. Few $CCR2\text{-}RFP^+$ cells were encountered in the saline solution-treated animals. (Scale bar: 100 μm.) (*B*) Stereological analysis of total hippocampal $Iba1^+$ cells showed more than threefold increase at the 3- and 14-d time points. There was an approximately twofold increase 1 d after KA injection ($n = 5$ for each condition; one-way ANOVA followed by Dunnett's post hoc tests). (*C*) Stereological analysis revealed ∼80,000 monocytes at the 3-d time point in the hippocampus. ANOVA followed by Tukey's post hoc tests revealed a significant difference of total hippocampal $CCR2\text{-}RFP^+$ monocytes between 1 d and 3 d as well as 3 d and 14 d (***$P < 0.001$; $n = 5$). (*D*) Most CCR2-RFP–expressing cells (red) were also $CD11b^+$ (green; arrows). A $CCR2\text{-}RFP^+$;$CD11b^-$ cell was occasionally encountered (arrowhead). Ramified $CCR2\text{-}RFP^-$ $CD11b^+$ microglia were also observed (asterisk). (Scale bar: 50 μm.) (*E*) All mice treated with KA showed a seizure severity score of at least 5.

by numerous short processes extending from the cell soma, that did not show detectable CCR2-RFP expression (Fig. 1*D*, asterisks). The highly ramified CCR2-RFP$^-$, CD11b$^+$ cells are likely to be activated brain-resident microglia. Given the scarcity of T cells in the CCR2$^+$ population, these findings provide evidence that, in addition to neuronal damage and inflammation, KA-induced SE can also cause CCR2$^+$ monocyte recruitment into hippocampal tissue. Furthermore, monocyte recruitment is not an immediate or early event. Rather, monocyte infiltration occurs between 1 and 3 d after SE onset, and is thus delayed relative to the onset of neurodegeneration and microglial activation.

Expression of CCL2 After SE. The chemokine CCL2 is a major ligand for CCR2 that recruits monocytes to inflamed tissues. To identify CCL2-expressing cells in the brain, CCL2::RFP transcriptional reporter mice were subjected to saline solution or KA (30 mg/kg) to induce SE and killed 1 or 3 d later. Use of this transcriptional reporter line allows for intracellular labeling and identification of cells expressing *Ccl2* mRNA (31). Notably, there was little staining for CCL2::RFP in the hippocampus of saline solution-treated mice. In contrast, CCL2::RFP staining was encountered in the hippocampus of mice 1 d after SE, and the CCL2::RFP staining was further enhanced 3 d after SE (Fig. 2*A*). One day after SE, we predominately observed two cellular structures expressing *Ccl2* mRNA, resembling blood vessels or highly ramified microglia (Fig. 2*A*, red asterisks, and *B*).

Iba1 staining was colocalized with the CCL2::RFP signal (Fig. 2*C*). Additionally, we detected CCL2::RFP$^+$ cells associated with cerebral blood vessels. To determine which vascular cell type expressed CCL2 mRNA, we stained endothelial cells with antibodies to CD31 (32), and used antibodies to CD206 to stain perivascular macrophages (33, 34), a myeloid cell type that resides in the perivascular space. There was no colocalization of endothelial CD31 and CCL2::RFP, but we observed strong colocalization of CD206 and CCL2::RFP (Fig. 2*C*), indicating that perivascular macrophages also expressed CCL2. CCL2 expression was not observed in astrocytes or neurons 1 d after SE. These findings indicate that microglia and perivascular macrophages initially express CCL2 at the 1-d time point after SE, before monocyte invasion. The numbers of hippocampal double-labeled CCL2-expressing Iba1$^+$ myeloid cells increased from an occasional double-positive cell in saline solution-treated mice to 52 cells per square millimeter of hippocampus 1 d after KA-induced SE, and 161 cells per square millimeter 3 d after SE (Fig. 2*D*).

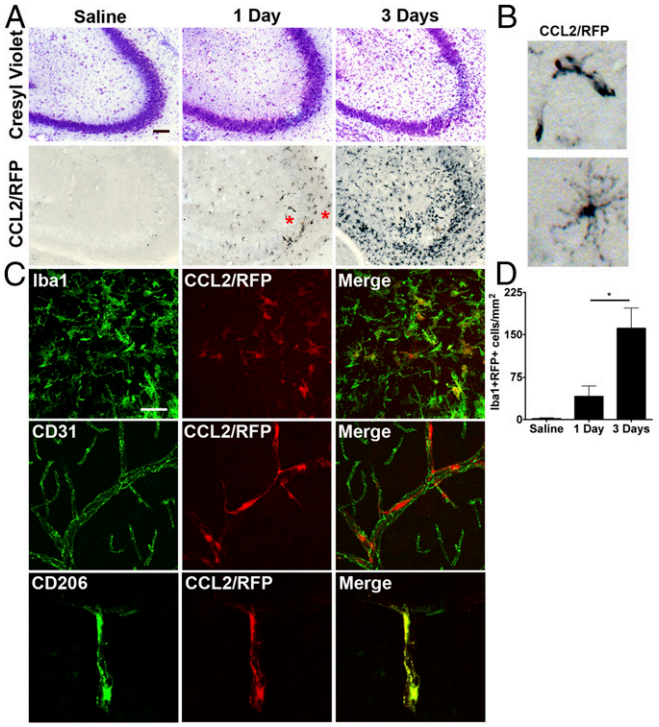

Fig. 2. Parenchymal Iba1$^+$ myeloid cells and perivascular macrophages express CCL2 at 1 and 3 d after kainate administration. CCL2::mRFP mice received KA (30 mg/kg, i.p.) or saline solution control injection and were killed 1 or 3 d later. (*A*) The mice subject to KA showed neuronal cell loss in the CA3 hippocampal region at the time points examined. Anti-RFP immunohistochemistry revealed CCL2-RFP$^+$ cells at the 1- and 3-d time points. At the 3-d time point, many CCL2-RFP$^+$ microglia are observed in the hippocampus. (Scale bar: 100 μm.) (*B*) Higher-magnification (~8× panels in Fig. 2*A*) images taken from cells at the 1-d time point revealing structures resembling blood vessels (right asterisk, *A*) and ramified microglia (left asterisk, *A*). (*C*) Representative images at 1 d showing Iba1 (microglia; *Top*), CD31 (endothelial cells; *Middle*), and CD206 (perivascular macrophages) staining with CCL2-RFP signal. Microglia and perivascular macrophages express CCL2. (Scale bar: 25 μm.) (*D*) Quantitative analysis of total hippocampal CCL2::RFP$^+$ myeloid cells (Iba1$^+$) in the hippocampus revealed a significant increase in the number of double-positive cells between the 1-d and 3-d time points (saline solution-treated, $n = 2$; 1-d, $n = 3$; 3-d, $n = 3$; $^*P = 0.047$, unpaired t test). The bars indicate the mean ± SEM.

***Ccr2* Deficiency Reduces the Number of Infiltrating Monocytes.** To interpret the phenotypic consequences of SE in the *Ccr2*$^{rfp/rfp}$ knockout mice, we first compared the temporal evolution of behavioral seizures in the deficient and heterozygous *Ccr2*$^{+/rfp}$ mice following KA. We found that both genotypes developed behavioral seizures with similar intensities and time courses (Fig. 3*A*). Three days after SE, we again examined brain tissue for neuronal degeneration, microgliosis, and brain invasion of circulating CCR2$^+$ monocytes. Neuronal damage and microglial activation were both encountered in KA-treated *Ccr2*$^{rfp/rfp}$ knockout mice and littermate *Ccr2*$^{+/rfp}$ controls. However, the numbers of Iba1$^+$ cells and CCR2$^+$ monocytes in the CCR2 knockout animals were reduced compared with the heterozygous controls (Fig. 3*B*). Indeed, stereological analysis of Iba1$^+$ cells in the hippocampus of KA-treated *Ccr2*$^{+/rfp}$ mice revealed approximately 1.7×10^5 cells 3 d after SE, compared with ~1.0×10^5 cells in *Ccr2* knockout (Fig. 3*C*). In addition, the number of CCR2$^+$ monocytes was reduced by 5.5×10^3 in the *Ccr2* knockout mice compared with the *Ccr2*$^{+/rfp}$ animals (Fig. 3*D*), supporting the idea that CCR2 mediates an important role in monocyte infiltration into the brain. Iba1 is expressed by brain-invading monocytes, but only after the monocytes have entered the brain and undergone maturation (35), so the reduced number of Iba1$^+$ myeloid cells in the CCR2-deficient mice (Fig. 3*C*) can be quantitatively accounted for by the loss of invading monocytes (Fig. 3*D*). Only rarely were CCR2-RPF–positive cells found to enter the brain in the *Ccr2* knockout animals. These cells were positive for the myelomonocytic marker CD11b, indicating that these cells were monocytes (Fig. 3*E*) that presumably were drawn into the brain in the absence of CCR2 signaling.

Pilocarpine-Induced SE also Causes Monocyte Brain Infiltration in a CCR2-Dependent Manner. Thus far, our experiments have used KA as the chemoconvulsant agent to cause SE. To exclude that monocyte infiltration is dependent on KA as an epilepsy model, we subjected *Ccr2*-sufficient and -deficient mice to pilocarpine, another widely used chemoconvulsant agent, and killed the mice 3 d later. Hippocampal tissue sections were then examined for CCR2-RFP–expressing monocytes. As expected, CCR2-RFP signal was not detected in the hippocampus of saline solution-treated *Ccr2* heterozygous mice (Fig. 4*A*). Similar to KA-treated mice, significant infiltration of CCR2-RFP$^+$ monocytes was observed in CCR2 heterozygous mice subject to pilocarpine-induced SE (Fig. 4*B*). In addition, monocyte infiltration was greatly reduced in *Ccr2* knockout mice experiencing pilocarpine-induced

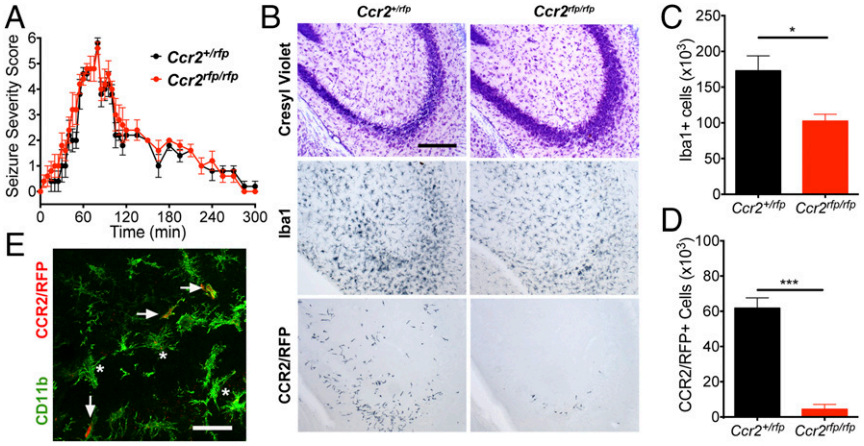

Fig. 3. *Ccr2* knockout mice have reduced numbers of Iba1$^+$ cells and CCR2-RFP$^+$ monocytes after SE. Two-month-old *Ccr2*$^{+/rfp}$ (n = 5) and *Ccr2*$^{rfp/rfp}$ (n = 4) mice received KA (30 mg/kg) and were monitored for seizure severity for 5 h. The mice were killed 3 d later. (*A*) The seizure severity was similar in the Ccr2 knockout mice compared with Ccr2 heterozygous animals after KA-induced SE. (*B*) At 3 d after SE, histological examination revealed that both genotypes showed neuronal damage in the CA3 region of the hippocampus as visualized by Cresyl violet staining, although damage appeared less pronounced in the *Ccr2*$^{rfp/rfp}$ mice. Analysis of adjacent sections showed that degeneration was accompanied by activation of Iba1$^+$ microglia in *Ccr2*$^{+/rfp}$ and *Ccr2*$^{rfp/rfp}$ mice. However, robust infiltration of CCR2-RFP–expressing monocytes was observed in only the *Ccr2*$^{+/rfp}$ mice. (Scale bar: 100 μm.) (*C*) Stereological analysis of total hippocampal Iba1$^+$ cells revealed a ~36% reduction in number of Iba1$^+$ cells in *Ccr2*$^{rfp/rfp}$ mice compared with *Ccr2*$^{+/rfp}$. (*D*) Stereological counts of CCR2-RFP–expressing monocytes showed a robust reduction in numbers of monocytes 3 d after SE in the *Ccr2*$^{rfp/rfp}$ mice compared with *Ccr2*$^{+/rfp}$ mice subject to SE. The bars indicate the mean ± SEM (*P = 0.025 and ***P < 0.001, unpaired t tests). (*E*) The occasional small CCR2-RFP–expressing cell in the *Ccr2*$^{rfp/rfp}$ mice was CD11b$^+$ (green; arrows) and is therefore likely to be a monocyte that has been called into the brain by a signal not requiring CCR2. The asterisks identify CCR2-RFP$^-$, CD11b$^+$ cells. (Scale bar: 50 μM.)

SE (Fig. 4*C*), to a similar degree observed in KA-treated mice (Fig. 3 *B* and *D*). These findings indicate that CCR2$^+$ monocytes infiltrate the brain after pilocarpine-induced SE and demonstrate that the CCR2-dependence of monocyte infiltration is independent of the chemoconvulsant agent used.

To examine the possibility that the appearance of monocytes in the brain after pilocarpine-induced SE can be simply attributed to an elevated number of monocytes circulating in the blood, whole blood was analyzed for steady-state levels of lymphocytes, monocytes, and neutrophils 3 d after SE. Notably, pilocarpine-induced SE did not change the blood levels of any leukocyte subtype examined, including monocytes (Fig. 4*D*). These findings indicate that a systemic action of pilocarpine-induced SE does not alter the number of circulating lymphocytes, monocytes, and neutrophils.

To gain further insights into diagnostic proteins expressed by myeloid cells after SE, we used flow cytometry. In addition to CCR2, Ly6C is also expressed at high levels in monocytes recruited to inflamed tissues (11, 36). The myeloid cell population was identified in brain 4 d after SE using CD11b (Fig. 4*E*). In these studies, Ly6C^{high} was used to identify brain-infiltrating blood-derived

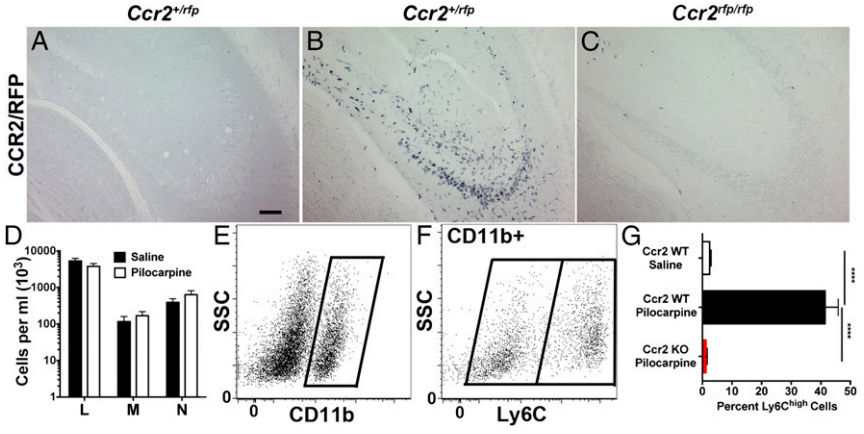

Fig. 4. Monocyte infiltration is robustly reduced in *Ccr2* knockout mice after pilocarpine-induced SE, and SE does not change blood levels of circulating leukocytes. Two-month-old *Ccr2*$^{+/rfp}$ and *Ccr2*$^{rfp/rfp}$ mice were pretreated with methylscopolamine (2 mg/kg, i.p.) and terbutaline (2 mg/kg, i.p.), and injected 20 min later with pilocarpine hydrochloride (280 mg/kg, i.p.) to induce SE or saline solution. SE was allowed to persist for 1 h before being interrupted by diazepam (10 mg/kg, i.p.). Three days after SE, histological examination of hippocampal tissue revealed brain infiltration of CCR2-RFP$^+$ monocytes in *Ccr2*$^{+/rfp}$ subject to pilocarpine (*B*), but not in *Ccr2*$^{+/rfp}$ animals that received saline solution (*A*) or in *Ccr2*$^{rfp/rfp}$ KO animals (*C*). (Scale bar: 50 μm.) (*D*) Blood values of lymphocytes (marked as "L"), monocytes ("M"), and neutrophils ("N") were not altered between saline solution-treated control and pilocarpine-treated mice (n = 6 per treatment). (*E* and *F*) Isolated brain myeloid cells from CCR2-sufficient mice were gated on CD11b (*E*) and divided into Ly6C^{low} and Ly6C^{high} populations (*F*). (*G*) Ly6C expression was quantified on the CD11b$^+$ population in mice 4 d after SE. One-way ANOVA followed by Tukey's post hoc test revealed significant differences between saline solution-treated *Ccr2*$^{+/+}$ and pilocarpine-treated *Ccr2*$^{+/+}$ mice as well as pilocarpine-treated *Ccr2*$^{+/+}$ and *Ccr2* KO animals (****P < 0.0001; n = 5 per group). The bars indicate the mean ± SEM.

monocytes, whereas Ly6C^{low} identified resident microglia (Fig. 4*F*). In saline solution-treated control animals, only 2% of CD11b$^+$ myeloid cells expressed high levels of Ly6C, in line with the finding that infiltrating CCR2$^+$ monocytes are rarely encountered in naïve brain, such that brain-resident microglia represent the predominant CD11b$^+$ population in the control brain (Fig. 4*G*). In comparison, 4 d after SE, ∼41% of the CD11b$^+$ myeloid cells expressed high levels of Ly6C, confirming the conclusion based on counting Iba1$^+$ and RFP$^+$ cells in the KA model that activated microglia and infiltrating monocytes are present in approximately equal numbers 3–4 d after SE. Finally, in stark contrast to CCR2-sufficient animals experiencing SE, pilocarpine-treated CCR2 knockout mice showed a 99% reduction in the percentage of Ly6C^{high}CD11b$^+$ cells, indistinguishable from saline solution-treated CCR2-sufficient controls (Fig. 4*G*).

Collectively, these results provide compelling evidence that the phenotypic characteristics of the brain's myeloid component are altered substantially after SE, wherein myeloid cells that infiltrate the brain express high levels of Ly6C, a canonical marker of peripherally derived monocytes (37, 38). Moreover, the appearance of Ly6C^{high}CD11b$^+$ myeloid cells after SE is reliant on CCR2.

Induction of IL-1β after SE Is Reduced in Monocyte-Poor Hippocampus. To gain insight into the contribution of CCR2$^+$ monocytes to inflammation after SE, we investigated the expression profile of a panel of inflammatory mediators in wild-type and *Ccr2* knockout mice 4 d after pilocarpine-inducted SE, when CCR2$^+$ monocytes have infiltrated hippocampal tissue (Fig. 4). Similar to KA-treated mice, pilocarpine administration resulted in nearly identical seizure severity scores regardless of *Ccr2* genotype (Fig. 5*A*). Quantitative real-time PCR (qRT-PCR) was performed on hippocampal tissue to measure the levels of five inflammatory mediators previously shown to be induced after SE (30, 39). The basal mRNA levels of these inflammatory mediators were nearly identical in saline solution-treated wild-type and *Ccr2* knockout animals (Fig. 5*B*). The mRNA levels of the inflammatory mediators, iNOS, CCL2, TNF-α, and IL-6, were all induced in CCR2-sufficient and -deficient animals at nearly identical levels. However, the induction of IL-1β was attenuated by ∼50% in the *Ccr2* knockout animals subject to pilocarpine-induced SE compared with wild-type mice ($P = 0.028$; Fig. 5*C*).

The Inflammatory Profile of Myeloid Cell Subsets. To evaluate the inflammatory response of brain-resident microglia and brain-infiltrating monocytes, mRNA levels of the proinflammatory cytokines IL-1β and TNF-α and the chemokine CCL2 were examined in FACS-purified myeloid cell populations obtained from brain 4 d after SE. Microglia and monocytes were isolated from brain homogenates 4 d after SE based on their differential expression of Ly6C and CD11b, wherein microglia are CD11b$^+$ and exhibit low levels of Ly6C, and brain-invading monocytes are also CD11b$^+$ but with higher levels of Ly6C than microglia (Fig. 4*F*).

In microglia harvested from brain 4 d after SE, the mRNA median levels of IL-1β were 16-fold higher than in microglia obtained from saline solution-treated control mice. By contrast, the median IL-1β level was elevated only threefold in brain-invading monocytes compared with blood monocytes ($P = 0.006$ for cell type comparison). TNF-α was also induced in microglia and monocytes from the SE brain. Monocytes showed lower induction of TNF-α compared with microglia (2.1- vs. 5-fold), but this did not reach statistical significance ($P = 0.067$) (Fig. 5*D*). The induction of CCL2 mRNA was approximately the same in monocytes (20-fold) and microglia (18-fold) (Fig. 5*D*).

Next, we normalized cytokine expression in microglia from the SE brain, brain-invading monocytes, and blood monocytes to that of microglia from saline solution-treated control mice.

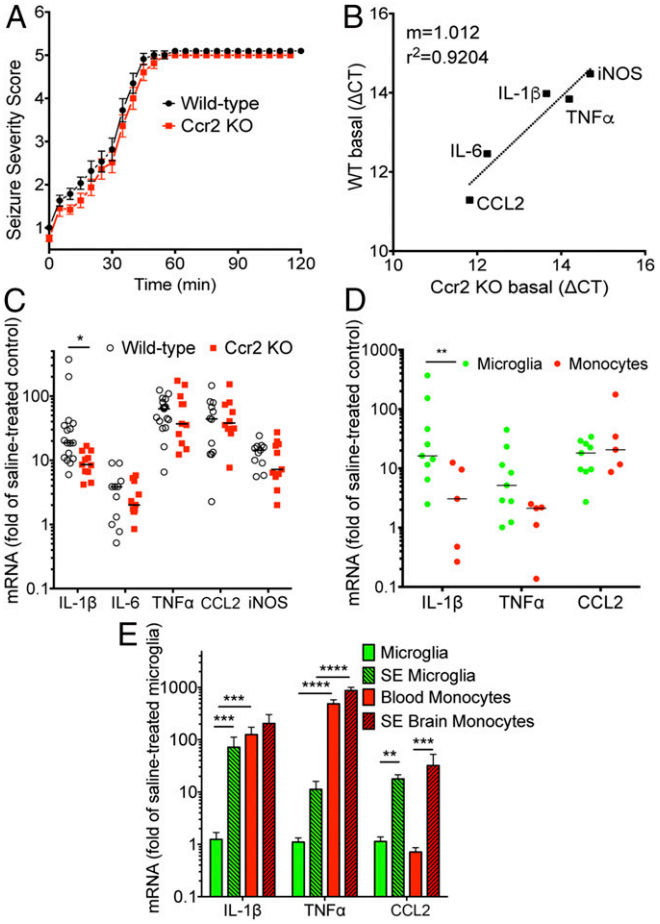

Fig. 5. Cytokine expression in hippocampus and myeloid cells after SE. (*A*) After pilocarpine injection, the behavioral seizure score was tabulated every 5 min until the seizure was interrupted by diazepam 1 h after SE onset in wild-type ($n = 14$) and Ccr2 knockout ($n = 11$). (*B*) The basal hippocampal levels of mRNA encoding inflammatory cytokines and mediators were similar in wild-type ($n = 6$) and *Ccr2*$^{rfp/rfp}$ ($n = 6$) animals injected with saline solution. (*C*) Median fold induction of the inflammatory cytokines and mediators in hippocampus is represented by the horizontal line and is plotted for wild-type ($n \geq 11$) and Ccr2 knockout ($n \geq 10$) mice 4 d after SE. Each symbol represents an individual mouse, with induction referenced to the mean of the appropriate saline solution-treated group. (*D*) Mice were subject to pilocarpine-induced SE for 1 h and killed 4 d later. mRNA was isolated from flow sorted CD11b$^+$Ly6C^{low} microglia ($n = 9$) and CD11b$^+$Ly6C^{high} brain-infiltrating monocytes ($n = 5$) and measured by qRT-PCR. The mRNA changes for SE-activated microglia were normalized to the mean of brain-resident microglia ($n = 5$) from saline solution-treated animals, whereas brain-infiltrating monocytes after SE were normalized to blood monocytes ($n = 5$). The horizontal line represents the median fold induction of each inflammatory mediator. Each symbol represents a population of myeloid cells prepared from an individual mouse. (*E*) mRNA changes for the myeloid cells were normalized to the mean of saline solution-treated microglia. Bars indicate the mean ± SEM (*$P = 0.028$, **$P < 0.01$, ***$P < 0.001$, and ****$P < 0.0001$ by one-way ANOVA with Sidák multiple-comparisons test).

IL-1β and CCL2 were significantly induced in microglia by SE (Fig. 5*E*). Interestingly, the mRNA levels of IL-1β were 125-fold higher in circulating blood monocytes than in control microglia, and TNF-α levels were 486-fold greater in blood monocytes (Fig. 5*E*). TNF-α levels were thus 79-fold greater in brain monocytes after SE compared with SE-activated microglia (Fig. 5*E*). These findings indicate that microglia and monocytes respond differently to SE. Whereas monocytes show little induction of IL-1β and TNF-α mRNA in response to SE and brain entry, activated microglia induce IL-1β and CCL2.

However, these results also indicate that the expression of IL-1β and TNF-α in circulating monocytes is much higher than that of activated microglia.

***CCR2* Deficiency Reduces SE-Induced BBB Opening.** Degradation of the BBB can occur after insults to the brain, including seizures (6, 40, 41). Serum albumin was detected by Western blot analysis in the PBS solution-perfused cortex four days following pilocarpine-induced SE in wild-type mice, compared with minimal albumin in saline solution-treated wild-type animals (Fig. 6). Strikingly, albumin extravasation into cortex was nearly abolished in *Ccr2* knockout mice after SE (Fig. 6). There was no significant difference in albumin levels in saline solution-treated wild-type mice compared with saline solution-treated *Ccr2* knockout mice. These findings suggest that monocyte infiltration in the days following SE further exacerbates BBB leakiness.

***CCR2* Ablation Enhances Weight Regain and Reduces Hippocampal Damage After SE.** We have previously shown that, during the 24 h following SE, rodents quickly lose 10–20% of their body weight and then gradually begin to recover in the following days (6, 8, 39). As expected, animals subject to SE lost ∼13% of their body weight in the 24 h after SE onset, independent of *Ccr2* genotype (Fig. 7*A*). Between 1 and 3 d after SE, animals of both genotypes began to regain weight. However, by the fourth day, the wild-type mice had regained only 33% of their initial weight lost, whereas the *Ccr2* knockout mice had improved significantly more, regaining 61% of their initial weight lost ($P < 0.05$ on day 4 and $P < 0.02$ for genotype comparison across days) (Fig. 7*A*).

SE produces a pattern of pyramidal neuron loss in adult rodents that can be quite variable from animal to animal (29, 42).

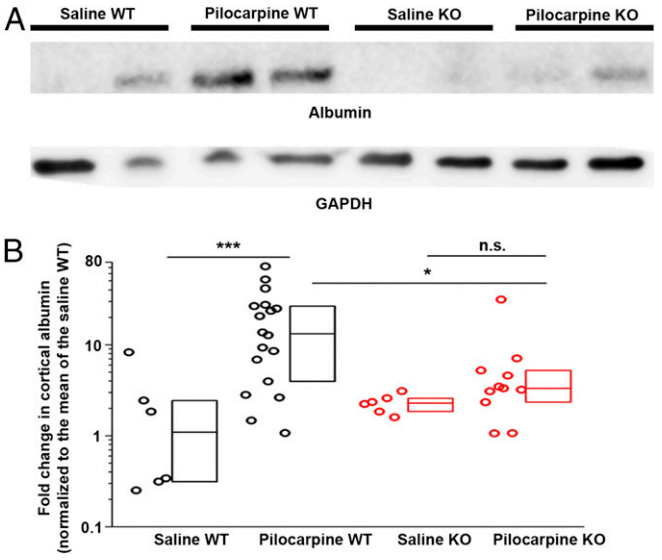

Fig. 6. The integrity of the BBB is maintained in *Ccr2* knockout mice after SE. (*A*) Serum albumin extravasation into the brain 4 d after pilocarpine SE was used to evaluate damage to the BBB. Albumin protein levels in cortical homogenates of saline-treated control wild-type ($n = 6$) and *Ccr2*-deficient ($n = 6$) mice and pilocarpine-treated wild-type ($n = 18$) and *Ccr2*-deficient ($n = 11$) mice were measured by Western blot with GAPDH as loading control. Two representative samples from each group are shown. (*B*) Normalized band intensity of the albumin protein relative to that of GAPDH and referenced to the mean albumin/GAPDH ratio in wild-type mice. The average log ratio of albumin was compared between each experimental group by one-way ANOVA with post hoc Sidák test with selected pairs (*$P = 0.043$ and ***$P < 0.001$). The fold-change normalized to the mean fold-change of the saline solution-treated wild-type group is plotted. Boxes represent the 25th/75th percentiles. The horizontal line in the boxes represents the median value.

We evaluated neurodegeneration in hippocampi from wild-type and *Ccr2* knockout mice 4 d after pilocarpine-induced SE. Fluoro-Jade B staining was not observed in hippocampus from saline solution-treated mice (Fig. S1). Although SE induced Fluoro-Jade B staining of injured neurons in the hippocampus in both wild-type and CCR2-deficient mice (Fig. 7*B*), the number of Fluoro-Jade B^+ neurons was reduced in the CA1 and CA3 subfields as well as the hilar region of the dentate gyrus in the CCR2 knockout (Fig. 7 *C* and *D*). On average, 130 stained CA3 neurons per section were counted in wild-type mice, whereas 69 stained neurons were identified in animals lacking CCR2 ($P < 0.05$). Likewise, when the total number of Fluoro-Jade B^+ hippocampal pyramidal neurons (CA1+CA3) was compared between the two genotypes, a significant 50% reduction in damaged neurons was observed (Fig. 7*D*) in the *Ccr2* knockout mice. The Fluoro-Jade B^+ neurons were colabeled with the TUNEL signal in both wild-type and CCR2-deficient mice (Fig. 7*E*), in agreement with our previous findings (9). In the wild-type mice, we found that 93% of the Fluoro-Jade B^+ CA1 and CA3 pyramidal neurons were $TUNEL^+$, and likewise 92% of the Fluoro-Jade B^+ pyramidal neurons in the *Ccr2* knockout mice were $TUNEL^+$. TUNEL staining was not encountered in saline solution-treated CCR2-sufficient and knockout mice (Fig. S1). We did not find evidence of cleaved caspase-3 staining in five hippocampal sections from each of three mice 4 d after pilocarpine-induced SE or in sections from one mouse killed 24 h after SE (Fig. S2). Despite the absence of cleaved caspase-3 staining in the hippocampus, we did find cleaved caspase-3 signal in damaged skeletal muscle, in line with previous reports (43).

These results reveal that the absence of CCR2 accelerates recovery of weight loss, safeguards against degradation of the BBB, and provides significant neuroprotection in the pilocarpine model of SE. Moreover, as CCR2 deficiency robustly limits blood-borne monocyte invasion into the brain, our findings suggest that infiltrating $CCR2^+$ monocytes exacerbate neuronal damage and the inflammatory consequences of SE.

Discussion

Here, we show that prevention of monocyte infiltration of the brain after SE is neuroprotective, reduces IL-1β expression in the hippocampus, seals the BBB, and modestly improves functional recovery of mice as assessed by weight regain. These results demonstrate the involvement of brain-invading $CCR2^+$ monocytes in the inflammatory response after 2–4 h of SE induced by KA or 1 h of SE induced by pilocarpine.

Blood-borne monocytes have been shown to infiltrate damaged or diseased brain tissue in animal models of other human neurological disease, such as the EAE model of multiple sclerosis (35), Alzheimer's disease (27, 28, 44), and traumatic brain injury (13, 45). Previous studies have also reported elevated numbers of peripheral immune leukocytes after epileptiform activity (46, 47). The current data confirm and extend these earlier findings in numerous notable ways.

Despite clear evidence of inflammation by altered microglia morphology 1 d after SE, hippocampal infiltration of $CCR2^+$ monocytes was delayed by at least 24 h, with nearly 8×10^5 monocytes invading the hippocampus by 3 d after SE. Interestingly, disruption of the BBB has been reported within 24 h of KA-induced SE (48), leading to extravasation of serum proteins. Our data indicate that early BBB disruption, per se, does not allow monocyte infiltration into the brain.

The $Ccr2^{rfp/rfp}$ mice used here have been used to study and visualize $Ly6C^{high}$ blood-borne monocytes, a subclass of innate immune myeloid cell that is recruited to inflamed tissues. This transcriptional mouse reporter line is advantageous because of the lack of dependable antibodies to detect CCR2-expressing cells, particularly in tissue sections (24). The CCR2 reporter line can also be used to convincingly discriminate brain-invading

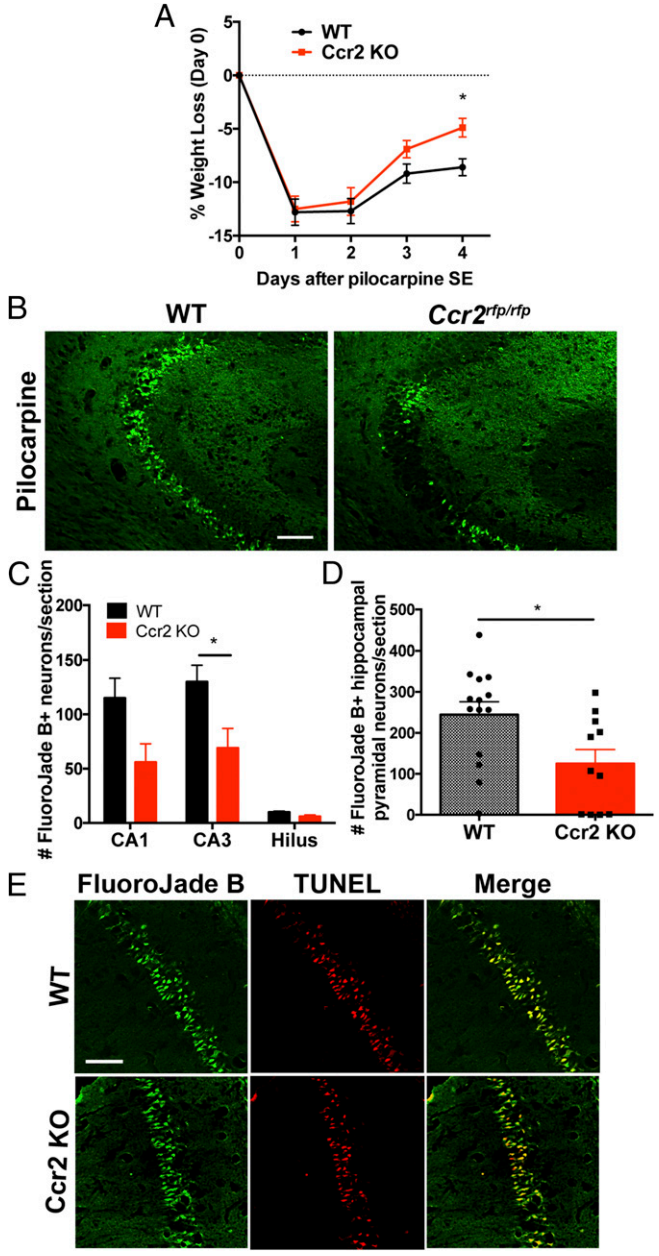

Fig. 7. Accelerated weight gain and neuroprotection in *Ccr2* KO after SE. (*A*) Effect of CCR2 deficiency on mouse body weight change after pilocarpine SE (n = 11–14 mice per time point, two-way ANOVA, interaction $P = 0.274$, time $P < 0.0001$, genotype $P = 0.02$, day 4 Bonferroni post hoc test; $^*P = 0.036$). (*B*) Fluoro-Jade B staining in hippocampal tissue sections 4 d after SE shows more injured neurons in the CA3 subfield of wild-type mice compared with Ccr2 knockout littermates. (Scale bar: 100 μm.) (*C*) A plot of the number of Fluoro-Jade B^+ cells in hippocampal cell layers. The bars indicate the mean ± SEM of each group ($^*P = 0.016$, unpaired t tests followed by Holm–Sidák test for multiple comparisons). (*D*) The number of Fluoro-Jade B^+ pyramidal neurons per hippocampal section is plotted for wild-type (n = 14) and Ccr2 knockout (n = 11; $^*P = 0.018$, unpaired t test). Each symbol represents the average number of Fluoro-Jade B^+ pyramidal neurons per section in each mouse. (*E*) Four days after SE, Fluoro-Jade B staining and TUNEL labeling are colocalized in CA1 pyramidal neurons in wild-type and *Ccr2* knockout mice. (Scale bar: 50 μm.)

monocytes from brain-resident microglia (16, 49). Indeed, histological examination of saline solution-treated $Ccr2^{+/rfp}$ animals revealed virtually no parenchymal CCR2-RFP expression in brain-resident microglia (Fig. 1). The *Ccr2* knockout mice confirmed that activated microglia also do not express CCR2 during an inflammatory response to SE, as CCR2-RFP expression was virtually abolished in the brain when monocyte infiltration was blocked by genetic ablation of CCR2, in agreement with the findings in EAE models (23).

However, there are limitations to the use of CCR2 reporter mice to track brain-infiltrating monocytes, including the down-regulation of CCR2 expression upon monocyte differentiation into tissue macrophages (50, 51). Our results show $CCR2^+$ monocytes in the brain 3 d after SE, but few are encountered at the 14-d time point. It is conceivable that the invading monocytes are still present in the brain, but are not detectable by using CCR2-RFP as a marker because of down-regulation. Another possibility is that the monocytes have died, as blood-borne myeloid cells do not engraft the brain on a long-term basis in EAE models (35). Nevertheless, the absence of CCR2-RFP^+ monocytes at the 14-d time point indicates that brain recruitment of blood-borne monocytes is transient, limited to the first few days after SE, and has ceased 2 wk after SE, suggesting the inflammatory processes responsible for and involving monocyte recruitment have resolved by the 2-wk time point.

Several ligands have been identified for CCR2, including CCL7, CCL8, CCL13, CCL16, and the most widely studied, CCL2 (52). CCL2 levels increase in the brain after SE (8, 9, 53–55), and SE-induced induction of CCL2 mRNA is rapid in hippocampal tissue, increasing more than 10-fold 30 min after SE onset and continuing to increase to nearly 100-fold 4 d after SE (39). Earlier studies reported that astrocytes are the cellular source of CCL2 after brain injury (56). We identified $Iba1^+$ microglia and $CD206^+$ perivascular macrophages as the major cellular sources of CCL2 at 1 d after SE. In light of these findings, one is prompted to ask how seizing neurons initiate myeloid cell expression of CCL2. One possibility is that neuron-released prostaglandin E_2, a product of cyclooxygenase-2 (COX-2), induces microglial CCL2 expression via EP2 receptors. Indeed, genetic removal of neuronal COX-2 or EP2 antagonism can mitigate the induction of CCL2 mRNA in the brain (6, 8, 9) or in purified microglia (57). Another possibility is that neuronal ATP release increases CCL2 in microglia via P2X7 receptors (58). However, additional work is required to test these ideas.

The fourfold increase in $Iba1^+$ cells 3 d after SE can be attributed to proliferation of the resident microglia and/or recruitment of the brain-invading monocytes. Mice lacking CCR2 had a reduced number of $Iba1^+$ cells and virtually complete prevention of brain recruitment of $Ly6C^+$ monocytes. The reduction in the number of $Iba1^+$ cells in the *Ccr2* knockout animals (Fig. 4*C*) compared with *Ccr2* heterozygous animals (~70,000 cells) is nearly equal to the number of invading monocytes in the CCR2-sufficient animals (Fig. 4*D*), suggesting that the reduced number of $Iba1^+$ cells is attributed mainly to the absence of $CCR2^+$ monocyte infiltration. However, we cannot rule out the possibility that microglia proliferation is mitigated in the absence of monocyte infiltrates. Regardless of the dominant mechanism, the absence of CCR2 profoundly altered the inflammatory milieu at the cellular level. The altered cellular environment was associated with selective attenuation of hippocampal IL-1β mRNA induction among the inflammatory mediators examined. Notably, IL-1β is proconvulsant and contributes to the underlying hyperactivity during febrile seizures (59). Additionally, blocking the generation of bioactive IL-1β inhibits electroencephalographic seizures (7), further endorsing the concept that inflammatory mediators contribute to the deleterious consequences of SE.

Even though *Ccr2* knockout mice displayed a similar behavioral seizure phenotype as their wild-type counterparts, hippocampal pyramidal neurons were protected from damage in the CCR2-deficient animals after SE. Nearly all of the Fluoro-Jade B^+ neurons are $TUNEL^+$, but cleaved caspase-3 was not observed. A previous study reported that <10% of $TUNEL^+$ neurons were

cleaved caspase-3 immunoreactive 24 h after intraamygdala KA model (60). These findings suggest that classical apoptosis is not the immediate cause of death for most pyramidal neurons. Pyroptosis, a cell death pathway involving activation of the inflammasome, is also typified by TUNEL$^+$ DNA breaks but caspase-3-independence (61).

The presence of CCR2$^+$ monocytes in the brain appears to exacerbate neuronal damage, but does not rescue the damage completely. Monocyte-derived IL-1β might promote neuronal death, as IL-1β signaling has been associated with neurotoxicity in vivo (62). Another noteworthy observation from our studies is that weight regain was enhanced in *Ccr2* knockout mice on the fourth day, but not at the earlier time points. We attribute the delayed beneficial effect on weight regain to the kinetics of monocyte infiltration, as monocytes enter the brain between 1 and 3 d after SE. Thus, the impact of inhibiting monocyte invasion would not be appreciated until after the monocytes enter.

Normalizing microglia and invading monocytes to their respective saline solution controls revealed that microglia showed a greater induction of the proinflammatory cytokine IL-1β compared with brain-infiltrating monocytes. However, the monocytes were not different from microglia in TNF-α and CCL2 induction. Insights into the responses of each myeloid cell type were also gleaned when control microglia were used as baseline for each myeloid cell population. In the absence of SE, blood monocytes showed 125-fold greater levels of IL-1β mRNA and 490-fold elevated levels of TNF-α compared with control microglia.

Total IL-1β induction in the hippocampus after SE was attenuated by 50% in CCR2-deficient mice. We attribute this reduction to the absence of monocytes in the brain, as the invading cells showed IL-1β mRNA levels 200-fold greater than control microglia. Thus, the two myeloid cell populations contribute an additive response in the SE models. Monocytes contribute to the inflammatory milieu in the brain just by their infiltration, even in the absence of proinflammatory cytokine induction, whereas, in microglia, the induced expression of cytokines contributes to neuroinflammation. This finding is in contrast to the antagonist response reported in EAE models (16, 63). A recent study reached similar conclusions on the role of invading monocytes after SE wherein monocytes have elevated levels of TNF-α and IL-1β when normalized to control microglia (64).

Extravasation of serum albumin into the brain after SE appears to promote the progression of epilepsy, as direct administration of albumin into the brain promotes inflammation and can result in development of spontaneous seizures (65). Moreover, degradation of the BBB has been demonstrated in humans after seizures by measuring the extravasation of serum albumin into the brain parenchyma (2). Here, we found that leakage of serum albumin into the brain via damaged BBB after pilocarpine SE was robustly blunted in *Ccr2*-deficient mice. The mechanism by which albumin extravasation into the brain is blunted in the absence of *Ccr2* remains unclear. The most straightforward explanation is that the influx of monocytes actively facilitates opening of the BBB, allowing albumin to enter the brain.

Our studies were designed to investigate the contribution of a subset of circulating myeloid cells after SE and to compare their response to brain-resident microglia. We found several benefits on disease outcome by preventing entry of CCR2$^+$ monocytes into the brain, including dampened inflammation, reduced number of Iba1$^+$ myeloid cells, ameliorated neuronal damage, reduced opening of the BBB, and accelerated weight regain. CCR2 antagonists are efficacious after traumatic brain injury (45) and have entered clinical trials for neuropathic pain treatment (66). We propose that selective targeting of myeloid cell subsets via chemokine receptors will allow manipulation of specific immune cell types in the brain after injury or during disease. Importantly, the delayed invasion of peripheral monocytes provides a window of opportunity for this therapeutic approach following SE.

Materials and Methods

Mice. In *Ccr2*$^{rfp/rfp}$ knockout mice, the *Ccr2* ORF was disrupted with a cDNA encoding RFP (24). *Ccr2*$^{rfp/rfp}$ mice were maintained on the Jackson Laboratory C57BL/6 (B6) background for at least nine generations. Female *Ccr2*$^{rfp/rfp}$ mice maintained on the Jackson Laboratory B6 background were bred to male Charles River FVB mice to generate F1 hybrid B6.FVB-*Ccr2*$^{+/rfp}$ mice. CCL2::mRFP transcriptional reporter mice express mRFP from the CCL2 promoter. The reporter gene was introduced into the mouse genome by using bacterial artificial chromosome technologies (31). Female CCL2::mRFP mice maintained on the Jackson Laboratory B6 background were bred to inbred FVB mice to generate F1 hybrid B6.FVB-CCL2::mRFP. For pilocarpine injections, *Ccr2*$^{rfp/rfp}$ mice were backcrossed to Charles River FVB mice for nine generations to create congenic N9 FVB-*Ccr2*$^{+/rfp}$ heterozygous mice. N9 FVB-*Ccr2*$^{+/rfp}$ mice were intercrossed to generate N9 FVB-*Ccr2*$^{rfp/rfp}$ knockout mice as well as N9 FVB-*Ccr2*$^{+/rfp}$ heterozygous and FVB-*Ccr2*$^{+/+}$ wild-type controls.

Male mice were used in all experiments. Mice were housed under a 12-h light/dark cycle with food and water ad libitum. All procedures and experiments were in compliance with protocols approved by the local animal use and care authorities and the institutional review board of the University of Tübingen as well as the guidelines of the animal care and use committee of Emory University.

KA Injection. KA was obtained from Sigma-Aldrich and was dissolved at 4 mg/mL in a physiological (0.9%) saline solution (pH 7.4) to generate a stock solution. The stock solution was diluted in 0.9% saline solution to create a working solution on the injection day. F1 B6.FVB-*Ccr2*$^{+/rfp}$ mice were weighed and injected with a single dose of KA at 30 mg/kg i.p. Control F1 B6.FVB-*Ccr2*$^{+/rfp}$ animals received 0.9% saline solution instead of KA. In mice, KA-induced seizures consisted of distinct motor behaviors, including forelimb clonus, loss of posture, rearing, and falling. Animals presenting these behaviors with increased seizure intensity, duration, and frequency after the injection of KA were declared to be in SE, which is characterized in the KA model by periodic rearing and falling accompanied by whole-body clonic seizures. Behavior was scored using a modified Racine scale as previously described (30). All mice that entered SE continued seizing for at least 60 min; seizures usually persisted for several hours.

Pilocarpine Injection. To minimize peripheral side effects of pilocarpine, mice were injected intraperitoneally with methylscopolamine and terbutaline (2 mg/kg each in 0.9% saline). After 20 min, pilocarpine hydrochloride (280 mg/kg in 0.9% saline solution, freshly prepared) was injected intraperitoneally in FVB-*Ccr2*$^{+/+}$ wild-type, FVB-*Ccr2*$^{+/rfp}$ heterozygous, or FVB-*Ccr2*$^{rfp/rfp}$ homozygous knockout controls to induce SE. Control mice of each genotype received methylscopolamine and terbutaline, followed by saline solution injection instead of pilocarpine. Seizures were classified as previously described (6, 67) as follows. A score of 0 represents normal behavior (walking, exploring, sniffing, grooming); a score of 1 represents immobile, staring, jumpy/curled-up posture; a score of 2 represents automatisms (repetitive blinking, chewing, head bobbing, vibrissae twitching, scratching, face-washing, "star-gazing"); a score of 3 represents partial body clonus, occasional myoclonic jerks, shivering; a score of 4 represents whole-body clonus, "corkscrew" turning and flipping, loss of posture, rearing and falling; a score of 5 (SE onset) represents nonintermittent seizure activity, stage 3 or 4 repeatedly; a score of 6 represents wild running, bouncing, and tonic seizures; and a score of 7 represents death. After 1 h of stage 5, SE was interrupted by diazepam (10 mg/kg, i.p.). Mice were fed moistened rodent chow, monitored daily, and injected with 5% (wt/vol) dextrose in lactated Ringer's solution (0.5 mL i.p.) when necessary.

Histology. Animals were deeply anesthetized with isoflurane and killed by cardiac perfusion with ice-cold PBS solution. Brains were removed from the cranium and fixed in 4% (wt/vol) paraformaldehyde (PFA) for 24 h followed by cryoprotection in 30% (wt/vol) sucrose in PBS solution. Brains were subsequently frozen in 2-methylbutane and coronally sectioned at 25 μm by using a freezing/sliding microtome. Immunohistochemical stainings were done by using the Vectastain Elite ABC Kits (Vector Laboratories). The following primary antibodies were used: rabbit polyclonal antibody to Iba1 (Wako), rabbit polyclonal antibody to RFP (Abcam), rabbit polyclonal antibody to mannose receptor CD206 (Serotec), and rabbit polyclonal to CD31 (Abcam). All antibodies were used at 1:1,000. Rabbit polyclonal antibody to cleaved caspase-3 (Cell Signaling) was used at 1:100. Cresyl violet staining was performed according to standard laboratory procedures.

Stereological Assessment of Cell Number. Numbers of Iba1- and RFP$^+$ cells were assessed on sets of every 12th systematically sampled 25-μm-thick, immunostained section through the hippocampus, typically yielding 8–10 sections per mouse as previously described (51). Analysis was performed with

the aid of the Stereologer software (Stereo Investigator 6; MBF Bioscience) and a motorized *x-y-z* stage coupled to a video microscopy system (Microfire color microscope camera; Optronics). The optical fractionator technique was used with 3D dissectors (area, 350 × 350 μm^2; height, 8; guard height, 2 μm; counting frame, 50 × 50 μm^2) (68). Iba1- or RFP^+ cells with complete soma within the dissector volume were counted.

Blood Cell Analysis. Whole blood was analyzed automatically by using the animal blood counter VetScan HM5 (ABAXIS).

Cell Isolation and Flow Cytometry. SE was induced with pilocarpine in $Ccr2^{rfp/rfp}$ and control $Ccr2^{+/+}$ animals maintained on the FVB background as described earlier. Four days after SE, the mice were perfused with Hanks' buffered salt solution, the brains were removed, and mononuclear cells were separated with a 30%/70% Percoll gradient as previously reported (69, 70). Single-cell suspensions from the brain were stained with anti–CD11b-PerCP (M1/70; BioLegend) and anti-Ly6C-FITC (AL-21; BD Pharmingen). Cells were analyzed on an LSR-II (BD) or sorted on a FACSAria II (BD) running Diva6. Data were analyzed with FlowJo software (Tree Star).

qRT-PCR. Four days after SE, FVB-$Ccr2^{+/+}$ wild-type and FVB-$Ccr2^{rfp/rfp}$ homozygous knockout mice, along with saline solution-treated FVB-$Ccr2^{+/+}$ and FVB-$Ccr2^{rfp/rfp}$ controls, were anesthetized deeply with isoflurane and perfused through the heart with PBS solution, and their brains were rapidly removed. The left hemisphere was fixed for 24 h in 4% PFA at 4 °C for Fluoro-Jade labeling. The hippocampus was dissected from the right half of the brain and immediately frozen on dry ice and stored at −80 °C for RNA isolation. Total RNA from mouse hippocampus was isolated by using TRIzol (Invitrogen) with the PureLink RNA Mini Kit (Invitrogen). RNA concentration and purity were measured by A260 value and A260/A280 ratio, respectively. First-strand cDNA synthesis was performed with 0.2 μg of total RNA, 200 U of SuperScript II Reverse Transcriptase (Invitrogen), and 0.5 μg random primers in a reaction volume of 30 μL at 42 °C for 50 min. The reaction was terminated by heating at 70 °C for 15 min. qRT-PCR was performed by using 8 μL of 50×-diluted cDNA, 0.1–0.5 μM of primers, and 2× iQ SYBR Green Supermix (Bio-Rad Laboratories), with a final volume of 20 μL, in the iQ5 Multicolor Real-Time PCR Detection System (Bio-Rad). Cycling conditions were as follows: 95 °C for 2 min followed by 40 cycles of 95 °C for 15 s and then 60 °C for 1 min. Melting curve analysis was used to verify single-species PCR product. Fluorescent data were acquired at the 60 °C step. The geometric mean of the cycle thresholds for β-actin, GAPDH, and HPRT1 was used as internal control of relative quantification (Table S1). Samples without cDNA template served as the negative controls.

RNA Extraction and Amplification from Sorted Myeloid Cell Populations. RNA was extracted from isolated microglia and monocytes using RNeasy spin columns (Qiagen) according to the manufacturer's instructions. RNA samples were analyzed with the nCounter Digital Analyzer (NanoString Technologies). Only samples with an RNA integrity value of at least 7 were selected for further analysis. RNA from 24 of 36 mice met this criterion. One round of poly-A RNA was performed on each sample by using Message*BOOSTER* cDNA synthesis kit for quantitative PCR (Epicentre Biotechnologies) following the manufacturer's instructions. Gene-expression analysis was performed as described earlier. The geometric mean of the cycle thresholds for β-actin, GAPDH, and HPRT1 was used as internal control of relative quantification (Table S2).

Western Blot Analysis of Albumin. Cerebral cortices from saline solution-perfused mice were homogenized in 20 volumes of RIPA buffer with protease and phosphatase inhibitors (Thermo Scientific). Brain homogenates were subsequently sonicated to shear DNA and centrifuged at 14,000 × *g* for 30 min at 4 °C to remove nuclei and cell debris. Brain protein was run on a 4–20% Mini-PROTEAN TGX Gel and electroblotted onto PVDF membranes (Millipore). Membranes were blocked for 1 h at room temperature with Odyssey blocking solution (Li-Cor), then incubated overnight at 4 °C with primary antibodies for albumin (1:1,000; Cell Signaling) and GAPDH (1:10,000; Calbiochem), followed by incubation with polyclonal IRDye secondary antibodies 680LT and 800CW (1:15,000; Li-Cor). The blots were imaged by using Li-Cor imaging systems using channels 700 and 800. Because all samples could not be run on the same gel, one sample was run on each blot for interblot normalization. The log value of the albumin/GAPDH ratio for each sample was determined. The average log ratio for selected groups was compared by ANOVA with post hoc Sidák adjustment. The fold-change for each group was plotted on a logarithmic scale.

Fluoro-Jade B Labeling. After overnight fixation, the left hemisphere was embedded in paraffin and coronally sectioned at 8 μm through the rostral hippocampus and mounted onto slides. Every 20th section for a total of approximately five to six sections from each half mouse brain was used for Fluoro-Jade staining to label degenerating cells. Sections were immersed in 0.06% potassium permanganate for 15 min with gentle agitation, rinsed for 1 min in distilled water, and then transferred to the Fluoro-Jade staining solution (0.0001% wt/vol in distilled water with 0.1% acetic acid) for 30 min with gentle agitation. Sections were rinsed with three 1-min changes of distilled water and air-dried. The slides were immersed in xylene and then coverslipped with D.P.X. mounting media (Sigma-Aldrich). Sections between bregma −1.34 and −2.40 were examined with a fluorescence microscope.

Following Fluoro-Jade B staining, images were obtained from three hippocampal areas (hilus, CA1, CA3). A researcher unaware of mouse genotype and experimental conditions counted the number of Fluoro-Jade–positive neurons in the hippocampus. Only positive neurons with a near-complete cell body shape and size were tabulated. Cell counts were expressed as the total number of Fluoro-Jade–positive cells per section.

For dual labeling with Fluoro-Jade B and TUNEL staining, sections were first processed for TUNEL labeling by using the in situ Cell Death Detection kit TMR red (Roche) and then processed for Fluoro-Jade B labeling. The modified protocol included immersion in 0.015% potassium permanganate for 10 min followed by incubation in 0.0001% Fluoro-Jade B solution for 8 min with gentle agitation. These modifications reduced the loss of TUNEL staining and minimized fluorescent bleed-through of Fluoro-Jade B labeling during microscopy.

Muscle Injury Model. Mice were anesthetized with intraperitoneal injection of 80 mg/kg ketamine and 5 mg/kg xylazine. Injury was induced in tibialis anterior muscles of anesthetized mice by injection of 25 μL of 1.2% $BaCl_2$. For analgesia, mice were injected subcutaneously with 0.1 mg/kg buprenorphine before and after muscle injury. Muscles were collected 7 d after injury depending on the experiment. Tissue was cryoprotected, frozen in Tissue Freezing Medium (Triangle Biomedical Sciences), and sectioned at 14 μm on a cryostat before mounting on a slide.

Data and Statistical Analysis. The results are expressed as mean values ± SEM. Statistical analysis was performed by using GraphPad Prism version 6 (GraphPad Software). One- or two-way ANOVA was used for comparison of selected means with post hoc Dunnett's test, Tukey's test, and Bonferroni or Sidák tests where appropriate. For Fluoro-Jade B counts, unpaired *t* tests followed by Holm–Sidák tests to correct for multiple comparisons were performed. For analysis of gene induction, the mean the ΔΔCT values was compared between selected groups. After statistical analysis, individual ΔΔCT values from each sample were converted to fold-change by 2^ΔΔCT, and the fold-change for each group was plotted on a logarithmic scale. For all analyses, the differences were considered to be statistically significant if $P < 0.05$.

ACKNOWLEDGMENTS. We thank A. Rojas, N. Lelutiu, C. Krueger, M. Tansey, C. Holler, and J. Odenthal for experimental advice and support; I. Charo for sharing the $Ccr2^{rfp/rfp}$ mice; and H. Choo for supplying injured muscle tissue. This research project was supported in part by the Emory University School of Medicine Flow Cytometry Core; Emory University Integrated Cellular Imaging Microscopy Core; Children's Healthcare of Atlanta; Emory University Pediatric Flow Cytometry Core; Cyberonics (N.H.V.); The Alexander von Humboldt Foundation (N.H.V.); a Roman Herzog Postdoctoral Fellowship of the Charitable Hertie Foundation (to J.J.N.); and National Institutes of Health, Office of the Director, National Institute of Neurological Disorders and Stroke Grants U01 NS05158, R21 NS074169, R01 NS097776, and P20 NS080185 (to R.D.).

1. Varvel NH, Jiang J, Dingledine R (2015) Candidate drug targets for prevention or modification of epilepsy. *Annu Rev Pharmacol Toxicol* 55:229–247.
2. van Vliet EA, et al. (2007) Blood-brain barrier leakage may lead to progression of temporal lobe epilepsy. *Brain* 130(pt 2):521–534.
3. Sakuma S, Halliday WC, Nomura R, Ochi A, Otsubo H (2014) Increased population of oligodendroglia-like cells in pediatric intractable epilepsy. *Neurosci Lett* 566:188–193.
4. Juhász C, et al. (2013) Successful surgical treatment of an inflammatory lesion associated with new-onset refractory status epilepticus. *Neurosurg Focus* 34(6):E5.
5. Vezzani A, Dingledine R, Rossetti AO (2015) Immunity and inflammation in status epilepticus and its sequelae: Possibilities for therapeutic application. *Expert Rev Neurother* 15(9):1081–1092.
6. Jiang J, et al. (2013) Inhibition of the prostaglandin receptor EP2 following status epilepticus reduces delayed mortality and brain inflammation. *Proc Natl Acad Sci USA* 110(9):3591–3596.
7. Maroso M, et al. (2011) Interleukin-1β biosynthesis inhibition reduces acute seizures and drug resistant chronic epileptic activity in mice. *Neurotherapeutics* 8(2):304–315.

8. Rojas A, Ganesh T, Lelutiu N, Gueorguieva P, Dingledine R (2015) Inhibition of the prostaglandin EP2 receptor is neuroprotective and accelerates functional recovery in a rat model of organophosphorus induced status epilepticus. *Neuropharmacology* 93:15–27.
9. Serrano GE, et al. (2011) Ablation of cyclooxygenase-2 in forebrain neurons is neuroprotective and dampens brain inflammation after status epilepticus. *J Neurosci* 31(42):14850–14860.
10. Levin JR, Serrano G, Dingledine R (2012) Reduction in delayed mortality and subtle improvement in retrograde memory performance in pilocarpine-treated mice with conditional neuronal deletion of cyclooxygenase-2 gene. *Epilepsia* 53(8):1411–1420.
11. Prinz M, Priller J, Sisodia SS, Ransohoff RM (2011) Heterogeneity of CNS myeloid cells and their roles in neurodegeneration. *Nat Neurosci* 14(10):1227–1235.
12. Mildner A, et al. (2009) CCR2+Ly-6Chi monocytes are crucial for the effector phase of autoimmunity in the central nervous system. *Brain* 132(pt 9):2487–2500.
13. Gyoneva S, et al. (2015) Ccr2 deletion dissociates cavity size and tau pathology after mild traumatic brain injury. *J Neuroinflammation* 12(1):228.
14. Fife BT, Huffnagle GB, Kuziel WA, Karpus WJ (2000) CC chemokine receptor 2 is critical for induction of experimental autoimmune encephalomyelitis. *J Exp Med* 192(6):899–905.
15. Izikson L, Klein RS, Charo IF, Weiner HL, Luster AD (2000) Resistance to experimental autoimmune encephalomyelitis in mice lacking the CC chemokine receptor (CCR)2. *J Exp Med* 192(7):1075–1080.
16. Yamasaki R, et al. (2014) Differential roles of microglia and monocytes in the inflamed central nervous system. *J Exp Med* 211(8):1533–1549.
17. London A, et al. (2011) Neuroprotection and progenitor cell renewal in the injured adult murine retina requires healing monocyte-derived macrophages. *J Exp Med* 208(1):23–39.
18. Shechter R, et al. (2009) Infiltrating blood-derived macrophages are vital cells playing an anti-inflammatory role in recovery from spinal cord injury in mice. *PLoS Med* 6(7): e1000113.
19. Ransohoff RM, Cardona AE (2010) The myeloid cells of the central nervous system parenchyma. *Nature* 468(7321):253–262.
20. Nimmerjahn A, Kirchhoff F, Helmchen F (2005) Resting microglial cells are highly dynamic surveillants of brain parenchyma in vivo. *Science* 308(5726):1314–1318.
21. Ajami B, Bennett JL, Krieger C, Tetzlaff W, Rossi FM (2007) Local self-renewal can sustain CNS microglia maintenance and function throughout adult life. *Nat Neurosci* 10(12):1538–1543.
22. Mildner A, et al. (2007) Microglia in the adult brain arise from Ly-6ChiCCR2+ monocytes only under defined host conditions. *Nat Neurosci* 10(12):1544–1553.
23. Mizutani M, et al. (2012) The fractalkine receptor but not CCR2 is present on microglia from embryonic development throughout adulthood. *J Immunol* 188(1):29–36.
24. Saederup N, et al. (2010) Selective chemokine receptor usage by central nervous system myeloid cells in CCR2-red fluorescent protein knock-in mice. *PLoS One* 5(10): e13693.
25. Geissmann F, Jung S, Littman DR (2003) Blood monocytes consist of two principal subsets with distinct migratory properties. *Immunity* 19(1):71–82.
26. Hsieh CL, et al. (2014) CCR2 deficiency impairs macrophage infiltration and improves cognitive function after traumatic brain injury. *J Neurotrauma* 31(20):1677–1688.
27. Mildner A, et al. (2011) Distinct and non-redundant roles of microglia and myeloid subsets in mouse models of Alzheimer's disease. *J Neurosci* 31(31):11159–11171.
28. El Khoury J, et al. (2007) Ccr2 deficiency impairs microglial accumulation and accelerates progression of Alzheimer-like disease. *Nat Med* 13(4):432–438.
29. Buckmaster PS, Dudek FE (1997) Neuron loss, granule cell axon reorganization, and functional changes in the dentate gyrus of epileptic kainate-treated rats. *J Comp Neurol* 385(3):385–404.
30. Rojas A, et al. (2014) The prostaglandin EP1 receptor potentiates kainate receptor activation via a protein kinase C pathway and exacerbates status epilepticus. *Neurobiol Dis* 70:74–89.
31. Jung H, et al. (2009) Visualization of chemokine receptor activation in transgenic mice reveals peripheral activation of CCR2 receptors in states of neuropathic pain. *J Neurosci* 29(25):8051–8062.
32. Bell RD, et al. (2010) Pericytes control key neurovascular functions and neuronal phenotype in the adult brain and during brain aging. *Neuron* 68(3):409–427.
33. Hawkes CA, McLaurin J (2009) Selective targeting of perivascular macrophages for clearance of beta-amyloid in cerebral amyloid angiopathy. *Proc Natl Acad Sci USA* 106(4):1261–1266.
34. Galea I, et al. (2005) Mannose receptor expression specifically reveals perivascular macrophages in normal, injured, and diseased mouse brain. *Glia* 49(3):375–384.
35. Ajami B, Bennett JL, Krieger C, McNagny KM, Rossi FM (2011) Infiltrating monocytes trigger EAE progression, but do not contribute to the resident microglia pool. *Nat Neurosci* 14(9):1142–1149.
36. Chu HX, et al. (2014) Role of CCR2 in inflammatory conditions of the central nervous system. *J Cereb Blood Flow Metab* 34(9):1425–1429.
37. Butovsky O, et al. (2012) Modulating inflammatory monocytes with a unique microRNA gene signature ameliorates murine ALS. *J Clin Invest* 122(9):3063–3087.
38. Butovsky O, et al. (2014) Identification of a unique TGF-β-dependent molecular and functional signature in microglia. *Nat Neurosci* 17(1):131–143.
39. Jiang J, et al. (2015) Therapeutic window for cyclooxygenase-2 related anti-inflammatory therapy after status epilepticus. *Neurobiol Dis* 76:126–136.
40. Marchi N, et al. (2007) Seizure-promoting effect of blood-brain barrier disruption. *Epilepsia* 48(4):732–742.
41. Zlokovic BV (2008) The blood-brain barrier in health and chronic neurodegenerative disorders. *Neuron* 57(2):178–201.
42. Buckmaster PS, Jongen-Rêlo AL (1999) Highly specific neuron loss preserves lateral inhibitory circuits in the dentate gyrus of kainate-induced epileptic rats. *J Neurosci* 19(21):9519–9529.
43. Hochreiter-Hufford AE, et al. (2013) Phosphatidylserine receptor BAI1 and apoptotic cells as new promoters of myoblast fusion. *Nature* 497(7448):263–267.
44. Lebson L, et al. (2010) Trafficking CD11b-positive blood cells deliver therapeutic genes to the brain of amyloid-depositing transgenic mice. *J Neurosci* 30(29):9651–9658.
45. Morganti JM, et al. (2015) CCR2 antagonism alters brain macrophage polarization and ameliorates cognitive dysfunction induced by traumatic brain injury. *J Neurosci* 35(2):748–760.
46. Borges K, McDermott DL, Dingledine R (2004) Reciprocal changes of CD44 and GAP-43 expression in the dentate gyrus inner molecular layer after status epilepticus in mice. *Exp Neurol* 188(1):1–10.
47. Zattoni M, et al. (2011) Brain infiltration of leukocytes contributes to the pathophysiology of temporal lobe epilepsy. *J Neurosci* 31(11):4037–4050.
48. van Vliet EA, Otte WM, Gorter JA, Dijkhuizen RM, Wadman WJ (2014) Longitudinal assessment of blood-brain barrier leakage during epileptogenesis in rats. A quantitative MRI study. *Neurobiol Dis* 63:74–84.
49. Umekawa T, Osman AM, Han W, Ikeda T, Blomgren K (2015) Resident microglia, rather than blood-derived macrophages, contribute to the earlier and more pronounced inflammatory reaction in the immature compared with the adult hippocampus after hypoxia-ischemia. *Glia* 63(12):2220–2230.
50. Sica A, et al. (1997) Bacterial lipopolysaccharide rapidly inhibits expression of C-C chemokine receptors in human monocytes. *J Exp Med* 185(5):969–974.
51. Varvel NH, et al. (2012) Microglial repopulation model reveals a robust homeostatic process for replacing CNS myeloid cells. *Proc Natl Acad Sci USA* 109(44):18150–18155.
52. Charo IF, Ransohoff RM (2006) The many roles of chemokines and chemokine receptors in inflammation. *N Engl J Med* 354(6):610–621.
53. Foresti ML, et al. (2009) Chemokine CCL2 and its receptor CCR2 are increased in the hippocampus following pilocarpine-induced status epilepticus. *J Neuroinflammation* 6:40.
54. Manley NC, Bertrand AA, Kinney KS, Hing TC, Sapolsky RM (2007) Characterization of monocyte chemoattractant protein-1 expression following a kainate model of status epilepticus. *Brain Res* 1182:138–143.
55. Turrin NP, Rivest S (2004) Innate immune reaction in response to seizures: Implications for the neuropathology associated with epilepsy. *Neurobiol Dis* 16(2):321–334.
56. Glabinski AR, et al. (1996) Chemokine monocyte chemoattractant protein-1 is expressed by astrocytes after mechanical injury to the brain. *J Immunol* 156(11): 4363–4368.
57. Quan Y, Jiang J, Dingledine R (2013) EP2 receptor signaling pathways regulate classical activation of microglia. *J Biol Chem* 288(13):9293–9302.
58. Shieh CH, Heinrich A, Serchov T, van Calker D, Biber K (2014) P2X7-dependent, but differentially regulated release of IL-6, CCL2, and TNF-α in cultured mouse microglia. *Glia* 62(4):592–607.
59. Dubé C, Vezzani A, Behrens M, Bartfai T, Baram TZ (2005) Interleukin-1beta contributes to the generation of experimental febrile seizures. *Ann Neurol* 57(1): 152–155.
60. Araki T, Simon RP, Taki W, Lan JQ, Henshall DC (2002) Characterization of neuronal death induced by focally evoked limbic seizures in the C57BL/6 mouse. *J Neurosci Res* 69(5):614–621.
61. Dingledine R, Varvel NH, Dudek FE (2014) When and how do seizures kill neurons, and is cell death relevant to epileptogenesis? *Adv Exp Med Biol* 813:109–122.
62. Rothwell N (2003) Interleukin-1 and neuronal injury: Mechanisms, modification, and therapeutic potential. *Brain Behav Immun* 17(3):152–157.
63. Vainchtein ID, et al. (2014) In acute experimental autoimmune encephalomyelitis, infiltrating macrophages are immune activated, whereas microglia remain immune suppressed. *Glia* 62(10):1724–1735.
64. Vinet J, et al. (2016) Microglia are less pro-inflammatory than myeloid infiltrates in the hippocampus of mice exposed to status epilepticus. *Glia* 64(8):1350–1362.
65. Ivens S, et al. (2007) TGF-beta receptor-mediated albumin uptake into astrocytes is involved in neocortical epileptogenesis. *Brain* 130(pt 2):535–547.
66. Biber K, Möller T, Boddeke E, Prinz M (2016) Central nervous system myeloid cells as drug targets: Current status and translational challenges. *Nat Rev Drug Discov* 15(2): 110–124.
67. Borges K, et al. (2003) Neuronal and glial pathological changes during epileptogenesis in the mouse pilocarpine model. *Exp Neurol* 182(1):21–34.
68. Long JM, et al. (1998) Stereological analysis of astrocyte and microglia in aging mouse hippocampus. *Neurobiol Aging* 19(5):497–503.
69. Cardona AE, Huang D, Sasse ME, Ransohoff RM (2006) Isolation of murine microglial cells for RNA analysis or flow cytometry. *Nat Protoc* 1(4):1947–1951.
70. Cardona AE, et al. (2006) Control of microglial neurotoxicity by the fractalkine receptor. *Nat Neurosci* 9(7):917–924.